A hybrid symmetry-PSO approach to finding the self-equilibrium configurations of prestressable pin-jointed assemblies

Yao Chen, **Jiayi Yan**, **Jian Feng**, and **Pooya Sareh**

Abstract. For pin-jointed assemblies with many members or self-stress states, the form-finding problem using conventional methods generally involves considerable computational complexities due to the large size of the solution spaces. Here, we propose an improved form-finding method for prestressable pin-jointed structures by combining symmetry-based qualitative analysis with particle swarm optimization. Expressed in the symmetry-adapted coordinate system, the nodal coordinate vectors of a structure with specific symmetry and topology are independently extracted from the key blocks of the small-sized force density matrices associated with rigid-body translations. Then, the first block of the equilibrium matrix is computed, in which the null space reveals integral self-stress states. Particle swarm optimization is introduced and adapted to find feasible prestress modes, where the uniformity and unilaterality conditions of the members are considered. Besides, the QR decomposition with column pivoting is adopted for efficient computations on the null space of these blocks. The QR decompositions of the small-sized blocks of the force density matrix and the equilibrium matrix are performed iteratively, to simultaneously find a stable self-equilibrium configuration and a feasible prestress mode. Representative examples show the presented method is computationally efficient and accurate for the form-finding of symmetric tensegrities and prestressed cable–strut structures.

1 Introduction

Prestressable pin-jointed structures generally contain a number of self-stress states and can be infinitesimally rigid. They are a new type of spatial structures with interesting configurations, as well as desirable characteristics such as light weight and foldability, where flexible cables and compression struts act as basic units [1,2]. Contrary to traditional spatial structures and reinforced concrete structures [3], a prestressable pin-jointed structure is generally not stable at the initial configuration when there is no prestress. Thus, initial prestresses in the members are essential for obtaining or enhancing structural stability [4]. On the condition that a prestressable pin-jointed structure reaches a stable self-equilibrium state by initial prestresses, the structure can be transformed into a free-standing tensegrity [5], a cable truss structure, or a cable dome structure (e.g., the well-known Levy cable dome [6]).

From a structural design perspective, finding a specific self-equilibrium configuration and/or feasible prestress distribution of the members (also known as form-finding analysis [7,8]) is the key to developing a novel prestressed structure. Therefore, form-finding of prestressable pin-jointed structures has attracted great

Yao Chen (✉), Jiayi Yan, Jian Feng
Key Laboratory of Concrete and Prestressed Concrete Structures of Ministry of Education, and National Prestress Engineering Research Center, Southeast University, Nanjing 211189, China
E-mail: chenyao@seu.edu.cn

Pooya Sareh
Creative Design Engineering Lab (Cdel), School of Engineering, University of Liverpool, London Campus, London, UK

attention from researchers in different fields, such as mathematics [9,10], biology [11,12], novel robotics, and engineering structures [13,14]. However, it is often difficult to simultaneously determine initial prestresses and geometric configurations because of the strong coupling between them [15,16]. Several methods of form-finding have been proposed by various scholars [15,17–20]. Based on the D'Alembert principle, Motro [2] extended the dynamic relaxation method—commonly used for membrane structures—into the form-finding of tensegrity structures. Zhang and Ohsaki [18] proposed an adaptive force density method for tensegrity structures, where the form-finding results are dependent on the given force densities. Koohestani and Guest [15] proposed a numerical form-finding method for tensegrity structures, in which the basic variables are the lengths of members in a Cartesian coordinate system. Based on the affine transformations of nodal coordinates, Masic et al. [21] developed an algebraic form-finding method for tensegrity structures. Connelly and Back [22] adopted a group representation theory to explain mathematical principles behind tensegrity structures and employed symmetry principles to systematically classify them. It was followed by the development of complementary- based analytic and group-theoretic approaches to simplify the form-finding procedure of prestressable pin- jointed structures [23–25].

On the other hand, metaheuristics have been applied to the formation of the structures [26,27]. Kaveh and Bakhshpoori [28] presented certain well-known algorithms in a practical implementation framework, where the MATLAB codes and some benchmark structural optimization problems are provided. Further, iterative methods and optimization algorithms have been successfully exploited to develop large-scale or irregular prestressable pin-jointed structures [29–31]. Tran and Lee [32] proposed an iterative form-finding method for cable–strut structures where the force density and equilibrium matrices could be repeatedly computed and updated for detecting self-equilibrium configurations. Li et al. [33] proposed a Monte Carlo form-finding method for irregular tensegrity structures. Using the ant colony algorithm, Chen et al. [16] developed a form-finding method for tensegrity structures in which nodal positions are given in advance and the connectivity pattern of the members is viewed as a design variable. More recently, Xu et al. [34] have combined the force density theory and the mixed integer nonlinear programming for the optimization of tensegrity structures, where the topology and force densities are taken as design variables. These form-finding methods apply considerably fewer constraints on the structures and find some feasible form-finding solutions by optimizing the global object functions. They are robust and applicable to structures with a single integral self-stress state or a small number of self-stress states. However, when the number of nodes and members increases, the required rank deficiencies of certain matrices and the unilaterality properties of the members (i.e., cables are in tension and struts are in compression) are often difficult to be guaranteed, especially for large-scale structures with many self-stress states. Then, the computational complexity of the involved form-finding process increases significantly, because the space to be searched for feasible solutions becomes much larger.

Besides, the inherent symmetry of symmetric structures is frequently underutilized during the iterative form- finding process. In fact, using symmetry not only reduces computational complexity, but also provides us with insightful qualitative results [23,35–37]. A recent study [24] has shown that rigid-body motions necessarily lie in the null space of several key blocks of the symmetry-adapted force density matrix. In addition, integral self- stress states always retain full symmetry and come from the first block of the symmetry-adapted equilibrium matrix [25]. Importantly, these fully symmetric self-stress states are necessary requirements for the stability of symmetric cable–strut structures [4], whereas their proper combination can generate a feasible prestress mode. Group theory and graph products have been verified to be simple and effective for structures with symmetry and regularity [38–42]. Consequently, the symmetry-based qualitative analysis and the optimization algorithm would be combined for the nonlinear form-finding of prestressable pin-jointed structures, to significantly reduce the solution space and enhance the robustness of the involved form-finding procedure.

Here, by exploiting both symmetry analysis and particle swarm optimization (PSO) algorithm, we propose an advanced form-finding method for prestressable pin-jointed structures. A practical advantage of this method is that the nodal coordinate vectors and integral self-stress states are accurately and iteratively extracted from the null space of certain key blocks by a small computational cost, according to the qualitative knowledge obtained from the symmetry analysis. To effectively evaluate the feasible prestress distribution and consider the uniformity and unilaterality conditions of members, a particle swarm optimization model is developed. Moreover, the QR decomposition with column pivoting is introduced to extract the null space of block matrices. During form-finding, certain blocks of the force density matrix and the equilibrium matrix—expressed in the symmetry-adapted coordinate system—are iteratively computed, to simultaneously find a stable self-equilibrium configuration and a feasible prestress mode.

2 Advanced form-finding of symmetric prestressable pin-jointed structures

2.1 Flowchart and improvements of the proposed form-finding process

According to the force density method [18,43], it is known that the self-equilibrium equation of a prestressable pin-jointed structure can be expressed with respect to nodal coordinates:

$$\boldsymbol{D}\boldsymbol{x} = \boldsymbol{0},\ \ \boldsymbol{D}\boldsymbol{y} = \boldsymbol{0},\ \ \boldsymbol{D}\boldsymbol{z} = \boldsymbol{0}, \tag{1}$$

where $\boldsymbol{x}$, $\boldsymbol{y}$, and $\boldsymbol{z}$ are the nodal coordinate vectors along the directions $\boldsymbol{x}$, $\boldsymbol{y}$, and $\boldsymbol{z}$, respectively, and $\boldsymbol{D}$ is known as the force density matrix [7,18] or the stress matrix [10,44]. In fact, the matrix $\boldsymbol{D}$ can be directly established by the force density of each member, given by

$$D_{ij} = \begin{cases} \sum\limits_{k\in\Omega} q_k & \text{if} \quad i = j \\ -q_k & \text{elseif member } k \text{ connects to nodes } i \text{ and } j \\ 0 & \text{otherwise} \end{cases} \tag{2}$$

where q_k denotes the force density of the member k connected to nodes i and j and describes the set of all members connected to node i. On the other hand, when the internal forces of the members are taken as variables, the self-equilibrium equation can be rewritten as

$$\boldsymbol{H}\boldsymbol{t} = \boldsymbol{0}, \tag{3}$$

where $\boldsymbol{H}$ is the equilibrium matrix and $\boldsymbol{t}$ is the internal force vector. The force density matrix $\boldsymbol{D}$ and the equilibrium matrix $\boldsymbol{H}$ are coupled to each other, as the matrix $\boldsymbol{H}$ is determined by the nodal coordinate vectors and the force density of a member k is dependent on the internal force $\boldsymbol{t}_k$,

$$\boldsymbol{q}_k = \boldsymbol{t}_k / l_k. \tag{4}$$

In Eq. (4), l_k is the length of the member k. For a self-equilibrated pin-jointed structure with at least one state of self-stress, the matrices $\boldsymbol{D}$ and $\boldsymbol{H}$ are necessarily singular. It can be noticed from Eqs. (1) and (3) that the null space of the matrix $\boldsymbol{D}$ contains independent modes of nodal coordinates, while that of the matrix $\boldsymbol{H}$ contains independent states of self-stress. Thus, on the basis of strong coupling between these two matrices, the nonlinear form-finding method can be utilized to iteratively compute the matrices $\boldsymbol{D}$ and $\boldsymbol{H}$. On condition that the requirement on the rank deficiencies of the two matrices is satisfied, a non-degenerate prestressable pin-jointed structure can be developed [15,18,45]. For clarity, Fig. 1a shows the kernel iterative calculation during the form-finding method. It keeps updating the matrices $\boldsymbol{D}$ and $\boldsymbol{H}$ and gets out of the iteration loop when a self-equilibrated and stable structure is obtained [45].

The reported form-finding process shown in Fig. 1a exhibits efficiency and accuracy for both tensegrity structures and prestressed cable–strut structures with a single configuration or a small number of self-stress states [45]. However, when the number of self-stress states or the dimension of the solution space rises, it is frequently difficult to compute the force densities (from the internal forces evaluated by the self-stress states) and the nodal coordinate vectors (extracted from potential vectors of the null space of $\boldsymbol{D}$), as shown by the dark gray areas in Fig. 1a.

To overcome these difficulties, an improved form-finding method is presented, where the basic and nonlinear iteration loop is illustrated in Fig. 1b. Based on the specific symmetry properties of the structure, the first block matrix of the symmetry-adapted equilibrium matrix is computed, of which the null space necessarily contains integral self-stress states with full symmetry. Then, the initial prestress mode and thus the force densities can be obtained by using PSO to find an optimized combination of the integral self-stress states. In addition, our previous study has shown that the rigid-body motions must be associated with certain irreducible representations of a symmetry group, and nodal coordinates can be extracted from the null space of three key blocks of the symmetry-adapted force density matrix [24].

According to Fig. 1b, the improved form-finding procedure using both PSO algorithm and symmetry contains eight steps:

Step 1 Define a certain symmetry group G for the input structure in advance and identify irreducible representations associated with rigid-body translations from group theory tables [24,46]

$$\Gamma_{\mathrm{T}\in\{x,y,z\}} = \Gamma^{(i)},\quad i \in [1, \mu], \tag{5}$$

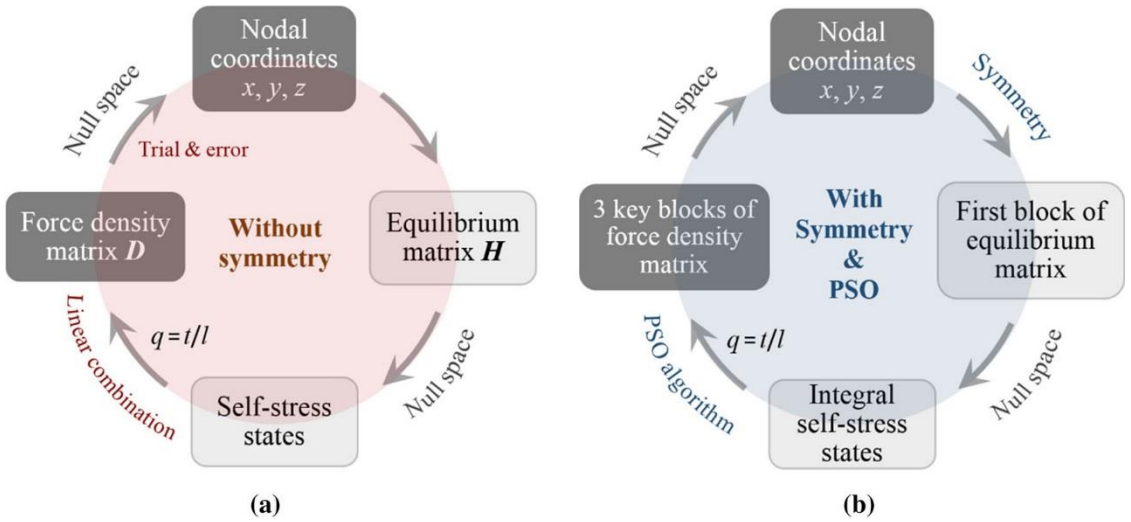

Fig. 1 Comparison between two different approaches to form-finding for prestressable pin-jointed assemblies: **a** form-finding process without symmetry; **b** a novel process based on symmetry and the PSO algorithm

where $\Gamma^{(i)}$ denotes the ith irreducible representation and μ is the total number of irreducible representations of the group G.

Step 2 For each independent symmetry operation $g \in G$, establish the node permutation matrix $\boldsymbol{N}_g$ and the member permutation matrix $\boldsymbol{M}_g$ by Eqs. (6) and (7):

$$[\boldsymbol{N}_g]_{ij} = \begin{cases} 1 & \text{if node } j \text{ moves to node } i \text{ under a symmetry operation } g \\ 0 & \text{otherwise} \end{cases} \tag{6}$$

$$[\boldsymbol{M}_g]_{kk'} = \begin{cases} 1 & \text{if member } k \text{ moves to member } k' \text{ under a symmetry operation } g \\ 0 & \text{otherwise} \end{cases} \tag{7}$$

Step 3 Compute the full symmetry subspace $\boldsymbol{V}_P^{(1-1)}$ for the external load vector and the full symmetry subspace $\boldsymbol{V}_t^{(1-1)}$ for the internal force vector, expressed as

$$\boldsymbol{V}_P^{(1-1)} = f\left(\sum_{g\in G} \Gamma_g^{(1-1)} \cdot (\boldsymbol{N}_g \otimes \boldsymbol{T}_g)\right), \quad \boldsymbol{V}_t^{(1-1)} = f\left(\sum_{g\in G} \Gamma_g^{(1-1)} \cdot \boldsymbol{M}_g\right), \tag{8}$$

where the function $f(\boldsymbol{X})$ is utilized to compute the orthogonal basis vector of the matrix X, $\otimes$ indicates the Kronecker product, $\boldsymbol{T}_g$ is a $d \times d$ transformation matrix to describe the symmetry operation g for a node, and d is the dimension of the given structure ($d = 2$ or 3). In a similar way, according to Eqs. (5) and (8), obtain the symmetry subspaces $\boldsymbol{V}_x$, $\boldsymbol{V}_y$, and $\boldsymbol{V}_z$ for the rigid-body translations along the x-, y-, and z-directions, respectively.

Step 4 Specify the initial force density vector by the inherent symmetry and certain types of the members,

$$\boldsymbol{q}_0 = \left\{ \underbrace{q_1 \cdots q_1}_{\text{type 1}}, \ldots, \underbrace{q_i \cdots q_i}_{\text{type } i}, \ldots, \underbrace{q_n \cdots q_n}_{\text{type } n} \right\}, \text{ where } \begin{cases} q_i \geq 0 & \text{for cables} \\ q_i < 0 & \text{for struts} \end{cases} \tag{9}$$

where n is the number of types of the members; then the force density matrix $\boldsymbol{D}$ can be computed through Eq. (2).

Step 5 Compute three key block matrices $\bar{\boldsymbol{D}}_x$, $\bar{\boldsymbol{D}}_y$, and $\bar{\boldsymbol{D}}_z$ of the symmetry-adapted force density matrix $\overline{\boldsymbol{D}}$,

$$\overline{\boldsymbol{D}}_x = \boldsymbol{V}_x^{\mathrm{T}} \boldsymbol{D} \boldsymbol{V}_x, \quad \overline{\boldsymbol{D}}_y = \boldsymbol{V}_y^{\mathrm{T}} \boldsymbol{D} \boldsymbol{V}_y, \quad \overline{\boldsymbol{D}}_z = \boldsymbol{V}_z^{\mathrm{T}} \boldsymbol{D} \boldsymbol{V}_z, \tag{10}$$

of which the null spaces $\overline{\boldsymbol{x}}$, $\overline{\boldsymbol{y}}$, and $\overline{\boldsymbol{z}}$ provide the solution space for the nodal coordinate vectors $\boldsymbol{x}$, $\boldsymbol{y}$, and $\boldsymbol{z}$ in the Cartesian coordinate system, given by

$$\boldsymbol{x} = \boldsymbol{V}_x\overline{\boldsymbol{x}}, \quad \boldsymbol{y} = \boldsymbol{V}_y\overline{\boldsymbol{y}}, \quad \boldsymbol{z} = \boldsymbol{V}_z\overline{\boldsymbol{z}}. \tag{11}$$

For a two-dimensional structure ($d = 2$), the symmetry subspace $\boldsymbol{V}_z$ associated with the irreducible representation Γ_z is not needed. Thereafter, involved computations for the vector $\boldsymbol{z}$ shown in Eqs. (9)–(10) can be neglected.

Step 6 Evaluate the first block $\bar{\boldsymbol{H}}^{(1-1)}$ of the symmetry-adapted equilibrium matrix $\boldsymbol{H}$,

$$\bar{\boldsymbol{H}}^{(1-1)} = (\boldsymbol{V}_P^{(1-1)})^{\mathrm{T}}\boldsymbol{H}\boldsymbol{V}_t^{(1-1)}, \tag{12}$$

of which the null space $\bar{\boldsymbol{S}}^{(1-1)}$ is utilized to compute the integral self-stress states S' with full symmetry, that is,

$$\boldsymbol{S}' = \boldsymbol{V}_t^{(1-1)}\bar{\boldsymbol{S}}^{(1-1)}, \text{ where } \bar{\boldsymbol{H}}^{(1-1)}\bar{\boldsymbol{S}}^{(1-1)} = \boldsymbol{0}. \tag{13}$$

Step 7 Employ the PSO algorithm to obtain the initial prestress mode $\boldsymbol{t}_0$ of the structure from the integral self-stress states $\boldsymbol{S}'$. (Detailed computation will be described in the next section.) Then, update the force density matrix $\boldsymbol{D}$ and the corresponding configuration.

Step 8 Check whether the terminal condition for the above-mentioned form-finding procedure is satisfied. If satisfied, terminate the iteration, whereas the corresponding stable configuration and the prestress mode are obtained. Otherwise, return to Step 5.

2.2 Rank-revealing QR algorithm for nodal coordinate vectors and integral self-stress states

The singular value decomposition technique can be considered to be one of the most common methods to obtain the null space or the generalized inverse of a matrix [45,47], because it is capable of computing both well-conditioned and singular matrices. Nevertheless, it is time-intensive, especially for large-sized matrices [48]. In fact, both the left-singular vectors and right-singular vectors, which require a large amount of computational effort, have little physical meaning during the form-finding process. Therefore, the rank-revealing QR algorithm is employed to extract the null space of involved matrices, which has been verified to be accurate for ill-conditioned sparse matrices and much faster than the singular value decomposition method [47,48].

To obtain the modes for nodal coordinates, the QR decomposition with column pivoting is performed on the key blocks $\overline{\boldsymbol{D}_x}$, $\overline{\boldsymbol{D}_y}$, and $\overline{\boldsymbol{D}_z}$ of the symmetry-adapted force density matrices at each iteration step. For instance, the transpose of the block $\overline{\boldsymbol{D}_x}$ can be decomposed into

$$\left(\overline{\boldsymbol{D}_x}\right)^{\mathrm{T}} = \boldsymbol{Q}_x\boldsymbol{R}_x\boldsymbol{P}_x^{\mathrm{T}}, \tag{14}$$

where $\boldsymbol{Q}_x$ is the orthogonal matrix, $\boldsymbol{P}_x$ is a permutation matrix such that the absolute values of the diagonal entries of the matrix $\boldsymbol{R}_x$ are in descending order ($|\boldsymbol{R}_{x11}| \geq |\boldsymbol{R}_{x22}| \geq \cdots \geq |\boldsymbol{R}_{xrr}| > 0$), and r is the rank of the matrix $\overline{\boldsymbol{D}_x}$.

Admittedly, the predicted configuration during the form-finding process might be significantly different from the expected one. Therefore, the corresponding force density matrix does not always satisfy the requirement of rank deficiency. In other words, the key block $\overline{\boldsymbol{D}_x}$, $\overline{\boldsymbol{D}_y}$, or $\overline{\boldsymbol{D}_z}$ at some iteration steps does not necessarily have null spaces. Then, there will be two possible cases during the nonlinear iterations:

Case I: The block matrix $\overline{\boldsymbol{D}_x}$ has null spaces, which is extracted from the matrix $\boldsymbol{Q}_x$

$$\boldsymbol{Q}_x = [\,\boldsymbol{Q}_{x1}\ \boldsymbol{Q}_{x2}\ \cdots\ \boldsymbol{Q}_{xr}\,|\,\overline{\boldsymbol{x}}\,], \text{ and } \overline{\boldsymbol{D}_x}\cdot\overline{\boldsymbol{x}} = \boldsymbol{0}, \tag{15}$$

where $\boldsymbol{Q}_{x1}$, $\boldsymbol{Q}_{x2}$, and $\boldsymbol{Q}_{xr}$, denote the first, second, and rth column of the matrix $\boldsymbol{Q}_x$, respectively. Then, the mode of the nodal coordinate vector $\overline{\boldsymbol{x}}$ can be obtained from Eq. (15).

Case II: The block $\overline{\boldsymbol{D}_x}$ has no null space (i.e., the matrices $\boldsymbol{R}_x$ and $\overline{\boldsymbol{D}_x}$ are non-singular). Thus, the geometric configuration predicted by the current force densities is impossible, which tends to degenerate into a plane

along the x-direction. Thereafter, the last column of $\boldsymbol{Q}_x$ is approximately taken as the nodal coordinate vector $\overline{\boldsymbol{x}}$ in the symmetry-adapted coordinate system, that is, $\overline{\boldsymbol{D}_x}\overline{\boldsymbol{x}} \approx \boldsymbol{0}$.

Note that the null space of the blocks $\overline{\boldsymbol{D}_y}$ and $\overline{\boldsymbol{D}_z}$ can be obtained in a similar way as described in Eqs. (14)–(15). Then, structural configurations can be repeatedly computed or approximated during the form-finding process.

On the other hand, the QR decomposition with column pivoting is employed on the first block $\bar{\boldsymbol{H}}^{(1-1)}$ of the symmetry-adapted equilibrium matrix at each iteration step, to obtain the integral self-stress states $\overline{\boldsymbol{S}}^{(1-1)}$. The transpose of the block $\bar{\boldsymbol{H}}^{(1-1)}$ can be decomposed into

$$\left(\bar{\boldsymbol{H}}^{(1-1)}\right)^{\mathrm{T}} = \boldsymbol{Q}_S \boldsymbol{R}_S \boldsymbol{P}_S^{\mathrm{T}}, \tag{16}$$

where $\boldsymbol{Q}_s$ is the orthogonal matrix, $\boldsymbol{P}_S$ is the corresponding permutation matrix, and $\boldsymbol{R}_S$ reveals the rank r_S of the matrix $\bar{\boldsymbol{H}}^{(1-1)}$. Also, the equilibrium matrix does not necessarily satisfy the requirement of rank deficiency, because the obtained prestress mode might be different from the final prestress mode. If the block $\bar{\boldsymbol{H}}^{(1-1)}$ has null space(s), then the matrix $\overline{\boldsymbol{S}}^{(1-1)}$ is exactly originated from the null space,

$$\boldsymbol{Q}_S = \left[\, \boldsymbol{Q}_{S1}\ \boldsymbol{Q}_{S2} \cdots \boldsymbol{Q}_{sr_s} \,|\overline{\boldsymbol{S}}^{(1-1)}\right], \text{ and } \bar{\boldsymbol{H}}^{(1-1)} \cdot \overline{\boldsymbol{S}}^{(1-1)} = \boldsymbol{0}, \tag{17}$$

where $\boldsymbol{Q}_{S1}, \boldsymbol{Q}_{S2}$, and $\boldsymbol{Q}_{Sr}$, denote the first, second, and r_Sth columns of the matrix $\boldsymbol{Q}_S$, respectively. Otherwise, the block $\bar{\boldsymbol{H}}^{(1-1)}$ has no null space. In other words, the structure cannot achieve a self-equilibrium state with the current nodal coordinates. The structural configuration tends to transform into another equilibrium state. In this case, the last column of $\boldsymbol{Q}_S$ is approximately taken as the integral self-stress state $\overline{\boldsymbol{S}}^{(1-1)}$ in the symmetry-adapted coordinate system, that is, $\bar{\boldsymbol{H}}^{(1-1)}\overline{\boldsymbol{S}}^{(1-1)} \approx \boldsymbol{0}$.

2.3 Terminal condition for nonlinear form-finding

As described in Step 8 and shown in Fig. 1b, the proposed nonlinear form-finding process does not stop until the terminal condition is satisfied. In fact, this terminal condition includes at least two aspects: the self-equilibrium condition and the stability condition. The self-equilibrium condition indicates that both the force density matrix and the equilibrium matrix of the structure need to satisfy the rank deficiency requirements, given by

$$n_D \geq d+1, \text{ and } s' \geq 1, \tag{18}$$

where n_D denotes the dimension of the null space of the force density matrix [15,18] and s' is the number of integral self-stress states [25]. Furthermore, the structural stability can be determined by the positive definiteness of the tangent stiffness matrix K_{T} [44,49,50], which is written as

$$\boldsymbol{K}_{\mathrm{T}} = \boldsymbol{H}\mathrm{diag}\left(\frac{E_k A_k}{l_k^0} - \boldsymbol{q}_{0k}\right)\boldsymbol{H}^{\mathrm{T}} + \boldsymbol{D} \otimes \boldsymbol{I}_d, \tag{19}$$

where E_k and l_k denote the Young's modulus and cross-sectional area of the member k, respectively, and $\mathbf{I}_d$ denotes the $d \times d$ identity matrix.

3 PSO model for evaluating feasible prestress modes during form-finding

It is known from Fig. 1 and Step 8 that the initial prestress mode is essential for detecting the final self-equilibrium configuration, which calls for repeated computations during form-finding. The existing methods generally evaluate the feasible prestress mode from the independent self-stress states [18,45], which takes much time and tends to obtain some unexpected configurations. Our previous study has proved that integral self-stress states necessarily retain full symmetry [25], which is a necessary stability condition for prestressable pin-jointed structures. Consequently, we can directly obtain the feasible prestress mode from the integral self-stress states $\boldsymbol{S}'$.

It is evident that, when there is a single integral self-stress state (i.e., $s' = 1$), the feasible prestress mode $\boldsymbol{t_0}$ is identical to $\boldsymbol{S}'$ or its inverse. That is,

$$\boldsymbol{t_0} = \boldsymbol{S}' \text{ or } \boldsymbol{t_0} = -\boldsymbol{S}' \text{ for } s' = 1. \tag{20}$$

In some cases, a prestressable structure has multiple integral self-stress states (i.e., $s' > 1$), especially for a large-scale structure with many members or complex geometry [30,51]. Then, the feasible prestress mode can be obtained from a linear combination of these integral self-stress states, given by

$$\boldsymbol{t_0} = \frac{\boldsymbol{S}_1'\alpha_1 + \boldsymbol{S}_2'\alpha_2 + \ldots + \boldsymbol{S}_{s'}'\alpha_{s'}}{\|\boldsymbol{S}_1'\alpha_1 + \boldsymbol{S}_2'\alpha_2 + \ldots + \boldsymbol{S}_{s'}'\alpha_{s'}\|_2} = \frac{\boldsymbol{S}'\boldsymbol{\alpha}}{\|\boldsymbol{S}'\boldsymbol{\alpha}\|_2}, \tag{21}$$

where the vector $\boldsymbol{\alpha} = [\,\alpha_1\ \alpha_2\ \cdots\ \alpha_{s'}\,]^{\mathrm{T}}$ contains the combination coefficients of the integral self-stress states and $\|\,\|_2$ describes the 2-norm of a vector. Thus, the proposed algorithm is applicable to symmetric structures with multiple states of self-stress (i.e., $s > 1$ or $s' > 1$).

3.1 Uniform prestress distribution of members

It is well known that the uniform prestress distribution of members is beneficial to structural design, construction, and maintenance of prestressed pin-jointed structures [50,52]. For instance, on the condition that the cross-sectional areas of most tension members (or compression members) are identical, the fabrication costs and complexity of the construction process would decrease significantly. Moreover, these members can hold an identical safety factor against member failure. To describe the uniformity of the initial prestress mode, an objective function $u(\boldsymbol{\alpha})$ is given by

$$u(\boldsymbol{\alpha}) = \sum_{k\in\Omega} (|\boldsymbol{t}_{0k}| - \overline{|\boldsymbol{t}_0|})^2, \tag{22}$$

where $|\boldsymbol{t}_{0k}|$ denotes the absolute value of the prestress of the member k and $\overline{|\boldsymbol{t}_0|}$ is the average of the absolute values of the prestresses. Then, the function $u(\boldsymbol{\alpha})$ is modified by

$$u'(\boldsymbol{\alpha}) = \frac{u(\boldsymbol{\alpha})}{u(\boldsymbol{\alpha}) + 1} \tag{23}$$

to guarantee the function $0 \le u'(\boldsymbol{\alpha}) < 1$.

3.2 The unilaterality condition of members

Importantly, the unilaterality condition of the members should be satisfied during form-finding, whereas the appointed cables should be in tension ($\boldsymbol{q}_k > 0$) and the struts should be in compression ($\boldsymbol{q}_k < 0$). However, the unilaterality condition is a strong constraint, which might lead to the divergence of the iterations. To avoid this case, this strong constraint is loosened and introduced to another object function $g(\boldsymbol{\alpha})$,

$$g(\boldsymbol{\alpha}) = \min\left\{\sum_{k\in\Omega}[\mathrm{sign}(\boldsymbol{t}_{0k}) - \mathrm{sign}(\boldsymbol{q}_{0k})],\ \sum_{k\in\Omega}[\mathrm{sign}(\boldsymbol{t}_{0k}) + \mathrm{sign}(\boldsymbol{q}_{0k})]\right\}, \tag{24}$$

where $\boldsymbol{q}_{0k}$ is the force density of the member k appointed in advance and the function sign $(\ ) = \pm 1$ (or 0 if no appointment) is utilized to identify the sign of the prestress (the force density, or the member type) of a member. For example, $\mathrm{sign}(\boldsymbol{q}_{0k}) = -1$ indicates that the member k has been appointed as a strut, while $\mathrm{sign}(\boldsymbol{q}_{0k}) = 1$ indicates that it is a cable. It should be mentioned that the latter expression in Eq. (24) is applicable to the case that the signs of all the prestresses are opposed to those of the initial force densities of the members.

3.3 Self-equilibrium condition for the structural configuration

To consider the self-equilibrium condition during nonlinear iterations, the rank deficiency constraint is also converted into a penalty function in the optimization model. Here, we denote a function $h(\boldsymbol{\alpha})$ as

$$h(\boldsymbol{\alpha}) = |n_D(\boldsymbol{\alpha}) - d - 1| \,. \tag{25}$$

In a similar way, the function $h(\boldsymbol{\alpha})$ is converted to

$$h'(\boldsymbol{\alpha}) = \frac{h(\boldsymbol{\alpha})}{h(\boldsymbol{\alpha}) + 1} \tag{26}$$

to guarantee the function $0 \leq h'(\boldsymbol{\alpha}) < 1$.

3.4 A multi-objective optimization model based on particle swarm optimization

The original problem of finding feasible prestress modes can be neatly transformed into a multi-objective optimization problem, where all the functions $u'(\boldsymbol{\alpha})$, $g(\boldsymbol{\alpha})$, and $h'(\boldsymbol{\alpha})$ need to be minimized. Here, we exploit a weight coefficient method to convert the original multi-objective problem into a single-objective problem. As a result, to obtain the feasible prestress mode from the integral self-stress states, the final objective function of the PSO model can be written as

$$F(\boldsymbol{\alpha}) = \omega_1 u'(\boldsymbol{\alpha}) + \omega_2 g(\boldsymbol{\alpha}) + \omega_3 h'(\boldsymbol{\alpha}), \tag{27}$$

where ω_1, ω_2, and ω_3 are weight coefficients. In fact, the objectives in Eq. (21) are not of the same status. Only the unilaterality condition of the members has to be strictly satisfied. Thus, the value of ω_2 should be the largest one among the three weight coefficients.

On the other hand, the particle swarm optimization (first introduced by Kennedy [53]) is a well-known optimization algorithm and has been successfully applied to the topology and geometry optimization of engineering structures [54,55]. This population-based meta-heuristic algorithm is inspired by the social and cooperative behavior of various species (e.g., birds flocking and insects swarming). At the beginning of the PSO algorithm, a series of particles are arbitrarily spread in the search space. In fact, these particles would become potential solutions to the optimization problem. To guarantee the quality of each candidate, the PSO algorithm keeps being instructed by the personal experience (*Pbest*) and overall experience (*Gbest*) evaluated by the objective function, and the current motion of the particles to determine their new positions in the search space. Then, more and more particles in the solution space move toward better positions. Gradually, the algorithm converges to an optimal solution [54].

To consider the uniformity and unilaterality conditions of the members and the self-equilibrium condition, the PSO algorithm is adopted for the feasible prestress mode of a prestressable pin-jointed structure, expressed as

$$\begin{array}{ll} \text{minimize} & F(\boldsymbol{\alpha}) \\ \text{subject to} & \boldsymbol{\alpha}_i \in [-1, 1], \ i \in [1, \ s'] \end{array} \tag{28}$$

Figure 2 gives the pseudocode of the hybrid symmetry–PSO approach for evaluating feasible prestress modes during form-finding and describes the above-mentioned optimization process.

4 Representative examples

In this section, several typical prestressable pin-jointed structures are investigated with the proposed method implemented in MATLAB. First, a simple 2D tensegrity is presented to describe the form-finding process using the hybrid symmetry–PSO approach. Then, two numerical examples of 3D cable–strut structures and cable domes are given to show the applicability of the proposed method to general structures with many members and integral self-stress states.

In the PSO models in these examples, the weight coefficients are taken as $\omega_1 = 1$, $\omega_2 = 20$, and $\omega_3 = 1$. These values are determined based on the importance of the functions, and a trial-and-error process to guarantee stable convergence and satisfactory efficiency [50]. Without loss of generality, the elastic modulus is taken as $E_c = E_s = 2000\,\text{MPa}$ for all the cables and struts; the cross-sectional areas for the cables and the struts are $A_c = 5\text{mm}^2$ and $A_s = 50\,\text{mm}^2$, respectively [56].

4.1 Two-dimensional C_{2v} symmetric tensegrity structure

Figure 3 shows a simple two-dimensional C_{2v} symmetric tensegrity structure ($d = 2$), which consists of six nodes, eight cables, and three bars. According to the predefined C_{2v} symmetry, the members are divided into five types. The diagonal cables ①–④ are classified into type c1, the horizontal cables ⑤–⑥ are type c2, the vertical cables ⑦–⑧ are type c3, the diagonal struts ⑨–⑩ are type s1, and the strut ⑪ is type s2.

There are $\mu = 4$ irreducible representations in the C_{2v} symmetry group. It can be deduced from group theory tables [46] that the rigid-body translation along the x-direction is associated with the third irreducible representation (i.e., $\Gamma_x = \Gamma^{(3)}$, while that along the y-direction is associated with the fourth irreducible representation (i.e., $\Gamma_y = \Gamma^{(4)}$). Thus, the symmetry subspaces associated with Γ_x and Γ_y can be obtained as given by

$$\boldsymbol{V}_x = f\left(-\boldsymbol{P}_{C_2^1} + \boldsymbol{P}_{C_2^2} - \boldsymbol{P}_{\sigma_x} + \boldsymbol{P}_{\sigma_y}\right) = \frac{1}{2} \times \begin{bmatrix} -\sqrt{2} & 0 & 0 & \sqrt{2} & 0 & 0 \\ 0 & 1 & -1 & 0 & -1 & 1 \end{bmatrix}^{\mathrm{T}}, \tag{29}$$

$$\boldsymbol{V}_y = f\left(-\boldsymbol{P}_{C_2^1} + \boldsymbol{P}_{C_2^2} + \boldsymbol{P}_{\sigma_x} - \boldsymbol{P}_{\sigma_y}\right) = \frac{1}{2} \times [0 \quad -1 \quad -1 \quad 0 \quad 1 \quad 1]^{\mathrm{T}}, \tag{30}$$

```
Compute integral self-stress states using symmetry;
Initialization for PSO
    Randomly initialize each particle;
    Evaulate quality of each particle and Gbest;
While (stopping criteria not satisfied)          % cycle loop
    Update velocity and position of each particle;
    For each particle
        Locally evaluate function value using Eq. (28) and symmetry;
        Update optimal position of each particle;
    End
    Update global optimal solution and position of the group;
End
Provide feasible prestress mode for a structure with specified symmetry.
```

Fig. 2 Pseudocode of the hybrid symmetry–PSO approach

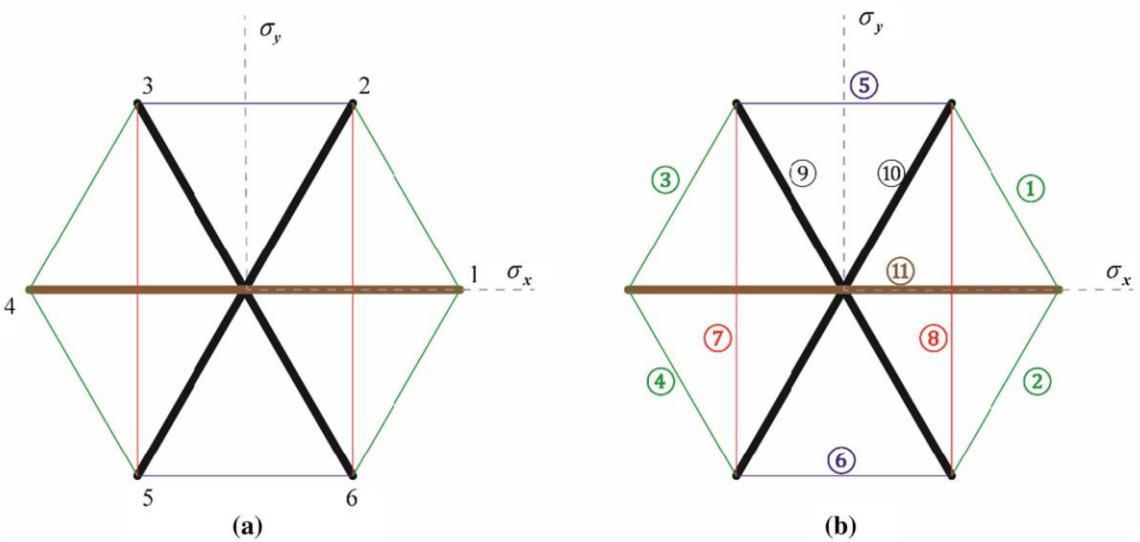

Fig. 3 A two-dimensional C_{2v} symmetric tensegrity structure

As shown in Fig. 3, this $G = C_{2v}$ symmetric structure should remain invariant under four independent symmetry operations: two rotations C_2^1 and C_2^2 and two mirror operations σ_x and σ_y along the x- and y-axes. That is, $C_{2v} = \{C_2^1,\ C_2^2,\ \sigma_x,\ \sigma_y\}$. The corresponding 2×2 transformation matrices for a general node under different symmetry operations are written as

$$\boldsymbol{T}_{C_2^1} = \begin{bmatrix} \cos(\pi) & -\sin(\pi) \\ \sin(\pi) & \cos(\pi) \end{bmatrix} = \begin{bmatrix} -1 & 0 \\ 0 & -1 \end{bmatrix},\quad \boldsymbol{T}_{C_2^2} = \begin{bmatrix} 1 & 0 \\ 0 & 1 \end{bmatrix},\quad \boldsymbol{T}_{\sigma_x} = \begin{bmatrix} 1 & 0 \\ 0 & -1 \end{bmatrix},\quad \boldsymbol{T}_{\sigma_y} = \begin{bmatrix} -1 & 0 \\ 0 & 1 \end{bmatrix}. \tag{31}$$

Based on Eqs. (8) and (25), the full symmetry subspace $\boldsymbol{V}_P^{(1-1)}$ corresponding to the external load vector is computed by

$$\begin{aligned} \boldsymbol{V}_P^{(1-1)} &= f\left(\boldsymbol{P}_{C_2^1} \otimes \boldsymbol{T}_{C_2^1} + \boldsymbol{P}_{C_2^2} \otimes \boldsymbol{T}_{C_2^2} + \boldsymbol{P}_{\sigma_x} \otimes \boldsymbol{T}_{\sigma_x} + \boldsymbol{P}_{\sigma_y} \otimes \boldsymbol{T}_{\sigma_y}\right) \\ &= \frac{1}{2} \times \begin{bmatrix} 0 & 0 & 0 & -1 & -1 & -1 & 0 & 0 & 0 & 1 & 0 & 1 \\ -\sqrt{2} & 0 & 0 & 0 & 0 & 0 & \sqrt{2} & 0 & 0 & 0 & 0 & 0 \\ 0 & 0 & -1 & 0 & 1 & 0 & 0 & 0 & 1 & 0 & -1 & 0 \end{bmatrix}^{\mathrm{T}}. \end{aligned} \tag{32}$$

Besides, the full symmetry subspace $\boldsymbol{V}_t^{(1-1)}$ corresponding to the internal forces of the members is obtained from Eq. (8),

$$\begin{aligned} \boldsymbol{V}_t^{(1-1)} &= f\left(\boldsymbol{R}_{C_2^1} + \boldsymbol{R}_{C_2^2} + \boldsymbol{R}_{\sigma_x} + \boldsymbol{R}_{\sigma_y}\right) \\ &= \tfrac{1}{2} \times \begin{bmatrix} 0 & 0 & 0 & 0 & 0 & 0 & 0 & 0 & -\sqrt{2} & -\sqrt{2} & 0 \\ 0 & 0 & 0 & 0 & 0 & 0 & -\sqrt{2} & -\sqrt{2} & 0 & 0 & 0 \\ 0 & 0 & 0 & 0 & 0 & 0 & 0 & 0 & 0 & 0 & 2 \\ 0 & 0 & 0 & 0 & -\sqrt{2} & -\sqrt{2} & 0 & 0 & 0 & 0 & 0 \\ -1 & -1 & -1 & -1 & 0 & 0 & 0 & 0 & 0 & 0 & 0 \end{bmatrix}^{\mathrm{T}}. \end{aligned} \tag{33}$$

Equation (33) shows that the nonzero entries of $\boldsymbol{V}_t^{(1-1)}$ are related to the classification of the members. At the beginning of the iterations, the initial force densities of the members are taken as

$$\boldsymbol{q}_0 = \{q_{c1} = 1,\ q_{c2} = 1,\ q_{c3} = 1,\ q_{s1} = -1,\ q_{s2} = -1\}. \tag{34}$$

To implement the proposed form-finding process, the 2×2 key block $\overline{\boldsymbol{D}_x}$ and the 1×1 key block $\overline{\boldsymbol{D}_y}$ of the symmetry-adapted force density matrix, as well as the 3×5 block matrix $\bar{\boldsymbol{H}}^{(1-1)}$ of the symmetry-adapted equilibrium matrix, are repeatedly evaluated and updated using Eqs. (10)–(13). After five iterations, a stable self-equilibrium configuration is found as shown in Fig. 4a. It can be noticed that the result meets the predefined symmetry and the unilaterality condition of the members. It shows the structure has $s' = 2$ integral self-stress states with full symmetry, and the obtained feasible prestress mode of this structure is

$$\boldsymbol{t} = \{t_{c1} = 0.1025,\ t_{c2} = 0.1025,\ t_{c3} = 0.3050,\ t_{s1} = -0.5076,\ t_{s2} = -0.1025\}. \tag{35}$$

In addition, the existing nonlinear form-finding method reported by Tran and Lee [32] is utilized for comparison, where the initial force densities are identical to those given by Eq. (34). The obtained configuration is shown in Fig. 4b. As far as the computational complexity is concerned, the reported method has to repeatedly deal with the original 11×12 matrix rather than the smaller-sized block matrices. More importantly, because of the lack of qualitative analysis, the reported method has to try the potential prestresses and nodal coordinates from all the null space through a trial-and-error process. On the contrary, the proposed method can effectively extract these vectors from certain blocks, which are associated with a specific symmetry and contain the expected vectors.

As shown in Fig. 4b, the symmetry of the self-equilibrium configuration obtained from the reported method is lower than the predefined symmetry C_{2v}. The structure is only rotationally symmetric along a twofold axis, without containing any mirror operations. Furthermore, the obtained prestress distribution does not satisfy the unilaterality condition of the members, because members 2, 3, 7, and 8 act as struts rather than cables. Strictly speaking, this structure is not a classical tensegrity structure, since each of its nodes is connected by two or three struts.

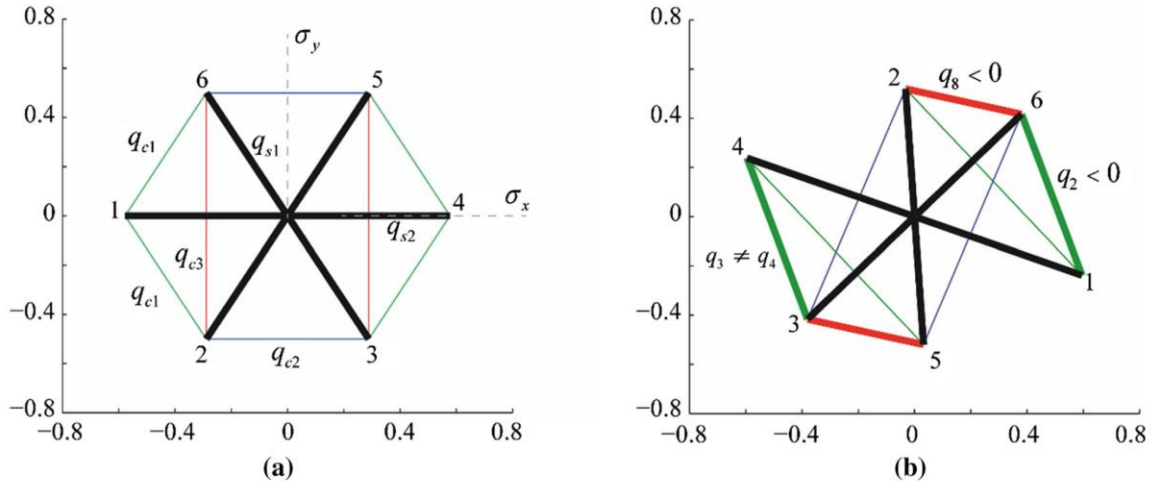

Fig. 4 Obtained configurations of the simple 2D tensegrity: **a** using the proposed form-finding process; **b** using the existing nonlinear form-finding method

It is worth noting that the proposed method is also applicable to asymmetric structures. However, when a structure is specified as asymmetric (i.e., its symmetry is of the lowest order $G = C_1$), the corresponding solution space is much larger than that of a symmetric structure. Therefore, in such cases, the proposed method has a limited advantage over the existing form-finding method.

Furthermore, to explore the effectiveness and adaptability of the proposed form-finding method based on symmetry analysis and PSO, different values for the initial force densities of the members are considered as inputs. The force density of each type of members is randomly determined to meet the unilaterality condition of the members. Interestingly, different force densities can lead to a series of stable configurations, which meet the conditions of members and the specific symmetry of the structure. For example, when the initial density vector is taken as

$$\boldsymbol{q}_0 = \{q_{c1} = 1/3,\ q_{c2} = 1/3,\ q_{c3} = 1/3,\ q_{s1} = -1,\ q_{s2} = -2/3\}\,, \tag{36}$$

it takes ten iteration steps to get the self-equilibrium configuration shown in Fig. 5a, where the feasible prestress mode $\boldsymbol{t}$ is given by

$$\boldsymbol{t} = \{t_{c1} = 0.0720,\ t_{c2} = 0.1977,\ t_{c3} = 0.4145,\ t_{s1} = -0.5202,\ t_{s2} = -0.1248\}\,. \tag{37}$$

If the initial density vector is

$$\boldsymbol{q}_0 = \{q_{c1} = 2,\ q_{c2} = 2,\ q_{c3} = 3,\ q_{s1} = -5,\ q_{s2} = -0.5\}\,, \tag{38}$$

then another self-equilibrium configuration, shown in Fig. 5b, is obtained after 21 iteration steps. The corresponding feasible prestress mode is

$$\boldsymbol{t} = \{t_{c1} = 0.0707,\ t_{c2} = 0.1026,\ t_{c3} = 0.4534,\ t_{s1} = -0.5163,\ t_{s2} = -0.1213\}\,. \tag{39}$$

Note that all the form-finding results shown in Figs. 4a and 5 are stable 2D tensegrity structures with the same connectivity pattern of members and the same predefined symmetry. Thus, this method provides an effective tool for designing cable–strut structures, where an appropriate force density can develop the desired configuration.

4.2 A D_4 symmetric cable–strut structure

Figure 6 shows the initial configuration and connectivity pattern of the members of a cable–strut structure [24,32], consisting of 12 pin joints, 16 cables, and 4 struts (illustrated by thick lines). The four nodes 9–12 are taken as the boundary nodes and constrained along the x-, y-, and z-directions. This structure is specified as $G = D_4$ symmetry. In other words, it is expected to remain invariant under four rotations with respect to

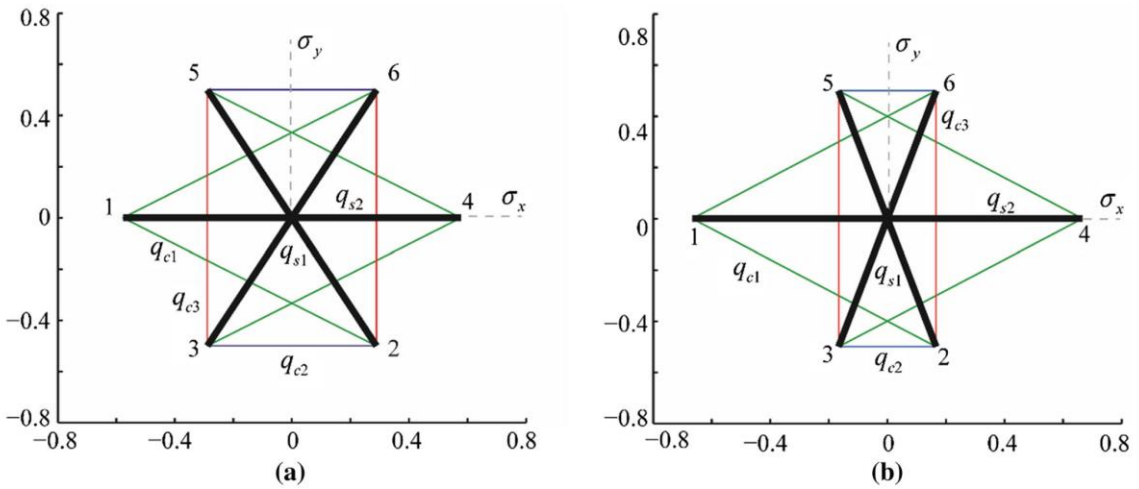

Fig. 5 Two typical self-equilibrium configurations induced by different initial force densities

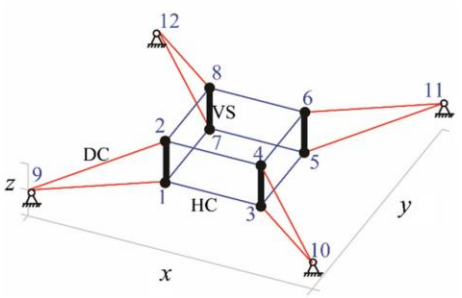

Fig. 6 A D_4 symmetric cable–strut structure

the same fourfold rotation axis and four twofold rotations with respect to four different symmetry axes. The specified symmetry allows the structural members to be divided into three types. As shown in Fig. 6, the eight diagonal cables connected to the boundary nodes are denoted by type DC, the other eight horizontal cables are denoted by type HC, and the vertical struts are denoted by type VS.

Mathematically speaking, the D_4 symmetry group contains $\mu = 6$ irreducible representations. Among these representations, the second one is necessarily associated with the rigid-body translation along the z-direction (i.e., $\Gamma_z = \Gamma^{(2)}$), while the fifth two-dimensional representation is associated with the rigid-body translations along the x- and y-directions (i.e., $\Gamma_x + \Gamma_y = \Gamma^{(5)}$). Thus, the symmetry subspaces $\boldsymbol{V}_x$, $\boldsymbol{V}_y$, and $\boldsymbol{V}_z$ corresponding to rigid-body translations can be obtained, which are, respectively, 12×3, 12×3, and 12×1 transformation matrices. Moreover, the full symmetry subspaces $\boldsymbol{V}_P^{(1-1)}$ and $\boldsymbol{V}_t^{(1-1)}$ for the external loads and the internal forces are obtained by Eq. (8), which are 24×3 and 20×3 matrices.

It should be noted that the computational efficiency of the proposed form-finding approach is demonstrated by this example. Once a set of initial force densities is given in advance, a stable self-equilibrium configuration can always be obtained through two iteration steps. This is because this structure contains a small number of types of members, and possesses only a single integral self-stress state (a PSO-based search for a feasible prestress mode is avoided). Some typical configurations of the cable–strut structure with different initial force densities are obtained and shown in Fig. 7. Table 1 lists the corresponding force densities values and the form-finding solutions, where the second and third columns show the obtained prestress modes $\boldsymbol{t}$ and the obtained force densities $\boldsymbol{q}$.

It can be noticed from Table 1 that the internal forces of the horizontal cables (type HC) and those of the diagonal cables (type DC) are independent, and the initial value of q_{HC}:q_{DC} determines the final self-equilibrium configuration. The initial force density of the struts q_{VS} has no effect on the final configuration, as verified by the results of the configurations in Figs. 7a, b. In fact, the form-finding solutions show that,

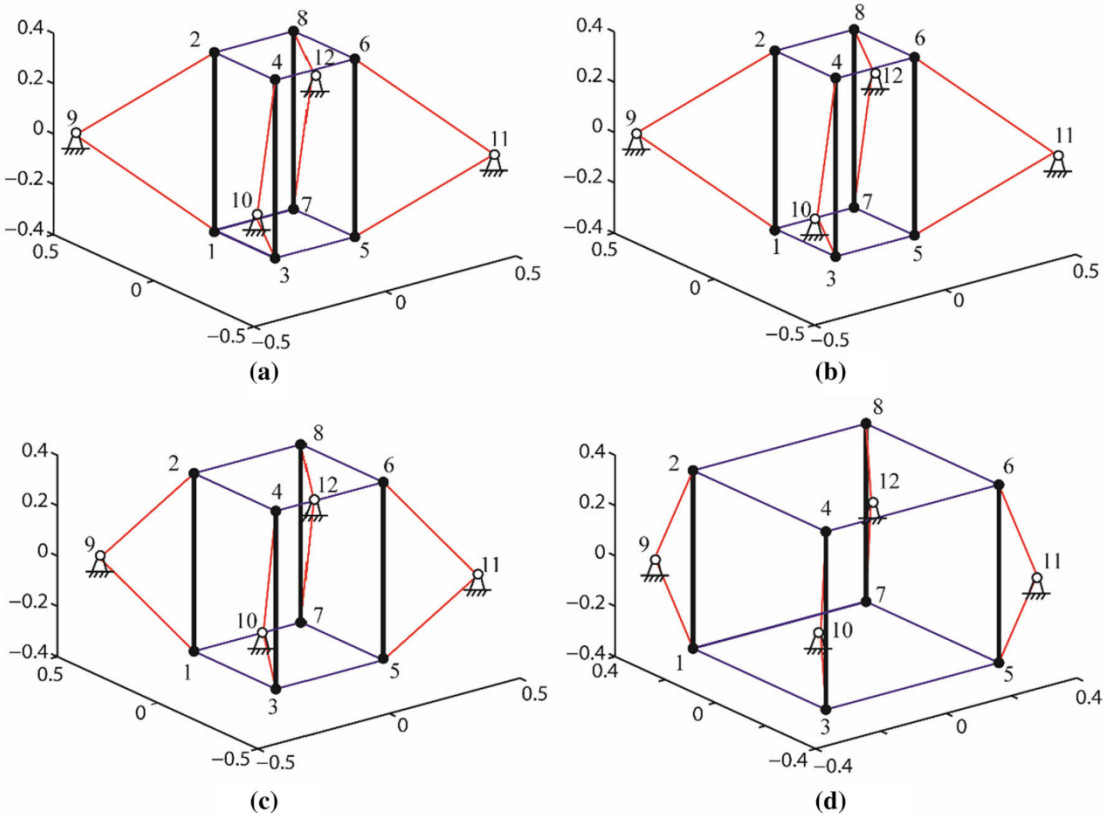

Fig. 7 Form-finding results of a D_4 symmetric cable–strut structure with different initial force densities

Table 1 Initial force densities and form-finding solutions of a D_4 symmetric cable–strut structure

Initial force density $\boldsymbol{q}_0$ q_{HC}:q_{DC}:q_{VS}	Obtained $\boldsymbol{t}$ t_{HC}:t_{DC}:t_{VS}	Obtained $\boldsymbol{q}$ q_{HC}:q_{DC}:q_{VS}	Configuration
1:1: − 1	1:1.837: − 1.173	1:1: − 0.5	Fig. 7a
1:1: − 20	1:1.837: − 1.173	1:1: − 0.5	Fig. 7b
1:2: − 1	1:2.236: − 1.732	1:2: − 1	Fig. 7c
1:8: − 1	1:5.523: − 5.339	1:8: − 4	Fig. 7d

regardless of the variations of the initial force densities, the force densities for the final configurations satisfy $q_{VS} = -0.5q_{DC}$. It agrees well with the results from the analytic form-finding method [24]

4.3 A Levy cable dome structure with C_{8v} symmetry

The initial topology of a classical cable dome structure of the well-known Levy type is studied [6], as shown in Fig. 8. This structure consists of 26 pin joints, 56 cables, and 9 struts. The outermost eight nodes are constrained along the three directions. As depicted in Fig. 8b, all the members have been divided into seven types, where DC1 and DC2 denote the two types of diagonal cables, RC1 and RC2 denote two types of ridge cables, HC denotes the hoop cables, and VS1 and VS2 denote the two types of vertical struts. In addition, the structure is expected to retain C_{8v} symmetry. Thus, its final configuration has to remain equivalent under eight rotational operations around the eightfold rotation axis and eight mirror operations.

In the C_{8v} symmetry group, there are $\mu = 7$ irreducible representations, where the first four representations are one dimensional and the others are two dimensional. Notably, the rigid-body translations along the z-direction are associated with the first irreducible representation (i.e., $\Gamma_z = \Gamma^{(1)}$), and the rigid-body translations

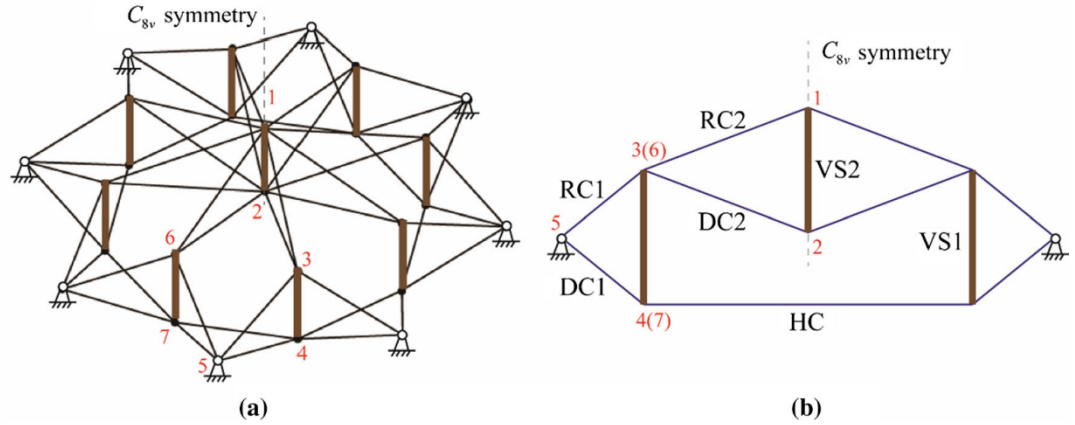

Fig. 8 A Levy cable dome structure with C_{8v} symmetry: **a** 3D view; **b** seven types of member and representative nodes are given in the section view

Table 2 Nodal coordinate vectors of the Levy cable dome obtained through nonlinear form-finding

Node	1	2	3	4	5	6	7
x	0	0	−0.1567	−0.1567	−0.3599	−0.2216	−0.2216
y	0	0	−0.1567	−0.1567	−0.1491	0	0
z	0.7227	0	0.1324	−0.2026	−0.0207	0.1324	−0.2026

along the x- and y-directions are associated with the fifth (two-dimensional) irreducible representation (i.e., $\Gamma_x + \Gamma_y = \Gamma^{(5)}$). It is important to point out that the vector $\mathbf{I} = [\,1 \quad 1 \quad \cdots \quad 1\,]^{\mathrm{T}}$ in the null space of the force density matrix is included in the null space of the first block matrix of the symmetry-adapted force density matrix, because it necessarily retains full symmetry. Therefore, to extract the desired nodal coordinates vector $\overline{\boldsymbol{z}}$ from the null space of the first block matrix $\overline{\boldsymbol{D}_z}$, the vector $\mathbf{I} = [\,1 \quad 1 \quad \cdots \quad 1\,]^{\mathrm{T}}$ needs to be eliminated [18,24]; that is, the rank deficiency of the block $\overline{\boldsymbol{D}_z}$ is at least 2.

Before the implementation of the proposed form-finding approach, certain symmetry subspaces for expressing the original problem in the symmetry-adapted coordinate system are obtained. The symmetry subspaces $\boldsymbol{V}_x$, $\boldsymbol{V}_y$, and $\boldsymbol{V}_z$ for the free nodes are 26×5, 26×3, and 26×3 matrices, respectively. The full symmetry subspace $\boldsymbol{V}_p^{(1-1)}$ corresponding to the external loads is a 54×6 matrix, while the full symmetry subspace $\boldsymbol{V}_t^{(1-1)}$ corresponding to the internal forces is a 65×7 matrix.

Given a set of initial force densities that satisfy the specified C_{8v} symmetry and the unilaterality condition of the members, a self-equilibrium configuration that guarantees structural stability can be obtained through nonlinear iterations. However, due to a large number of members and self-stress states of the Levy cable dome, the random force densities of the members frequently cause the strut members VS1 to be inclined. After a series of calculations, the initial force densities of the members with types RC2, DC2, and HC should be within a certain range, and a few reasonable Levy cable dome structures can be obtained by arbitrarily changing the force densities of the other members. For example, when the initial force densities are taken as

$$q_{\mathrm{RC1}}{:}q_{\mathrm{DC1}}{:}q_{\mathrm{RC2}}{:}q_{\mathrm{DC2}}{:}q_{\mathrm{HC}}{:}q_{\mathrm{VC1}}{:}q_{\mathrm{VC2}} = 1{:}1{:}2{:}2{:}3{:}-1.5{:}-1, \tag{40}$$

the proposed approach takes only eight iteration steps to find a stable structural configuration. The obtained nodal coordinate vectors for typical nodes (Fig. 8) of the Levy cable dome are listed in Table 2. The corresponding configuration and the feasible prestress distribution are illustrated in Fig. 9.

Furthermore, Fig. 10 shows four typical configurations of the Levy cable dome obtained at steps 2, 5, 6, and 8 during form-finding. It can be observed from Fig. 10 that although the structure cannot satisfy the self-equilibrium condition and the unilaterality condition of the members during the nonlinear iterations, the configuration obtained at each step retains the specified C_{8v} symmetry. It indicates that this method is effective in finding stable configuration while retaining full symmetry. During the iterations, the blocks, the original force density matrix, and the equilibrium matrix are gradually modified to meet the condition for rank deficiency. Finally, a stable structural configuration with the predefined C_{8v} symmetry can be effectively obtained.

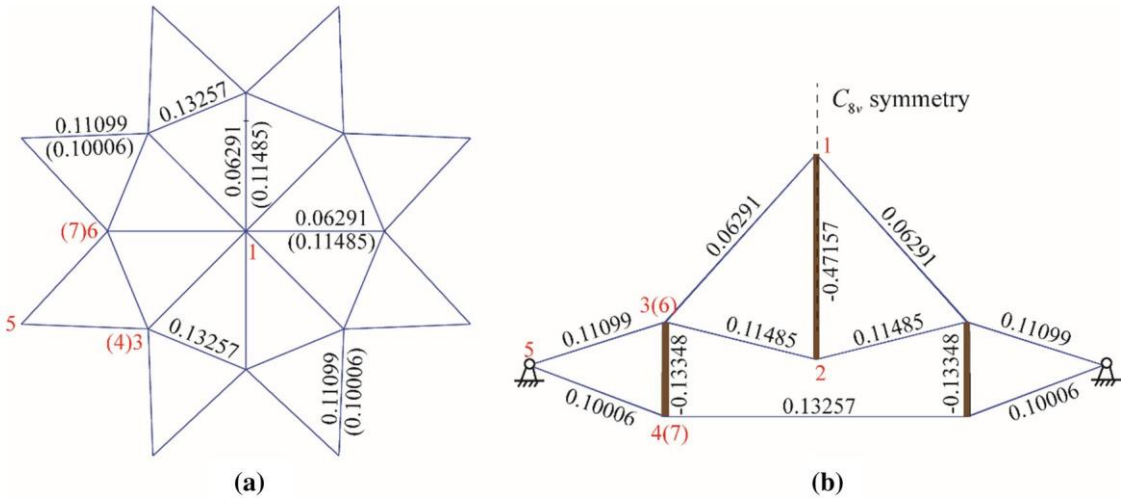

Fig. 9 Obtained self-equilibrium configuration and prestress distribution of the Levy cable dome: **a** plan view; **b** section view

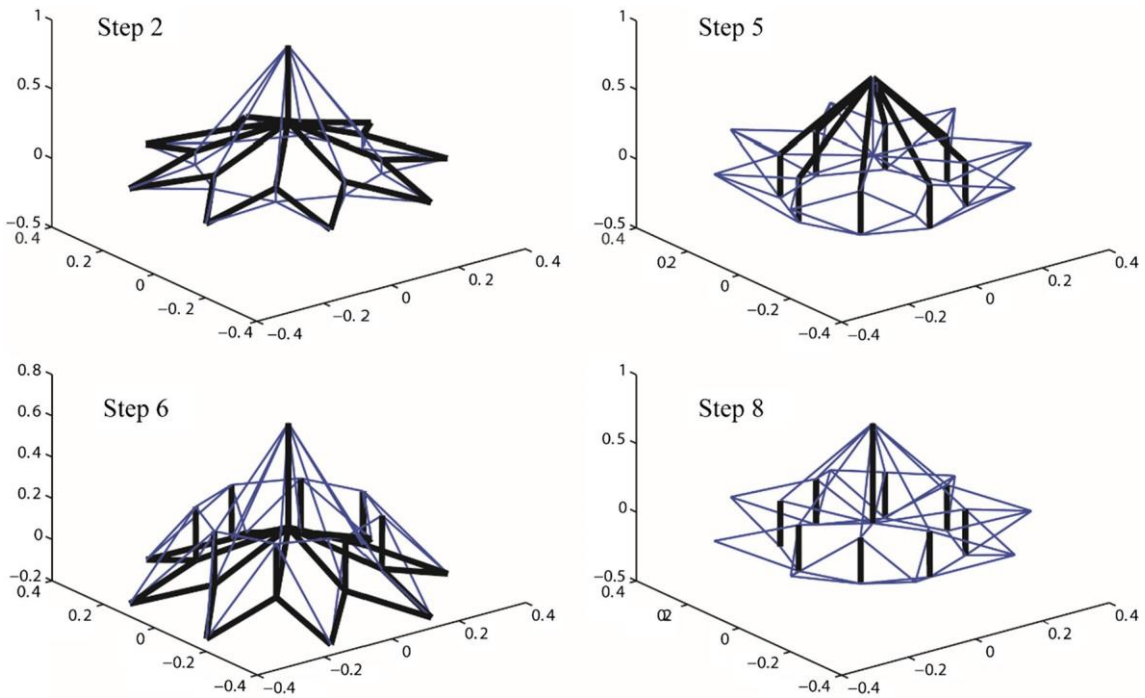

Fig. 10 Typical configurations of the Levy cable dome during form-finding

5 Conclusions

This paper presented an improved form-finding method of symmetric prestressable pin-jointed structures. We demonstrated that by combining a specified symmetry with a PSO algorithm, the proposed method can effectively find both the stable self-equilibrium configuration and the feasible prestress mode for a prestressable structure. During form-finding, a PSO model for evaluating the prestress mode of a structure with multiple self-stress states is developed. Several numerical examples with different symmetries were presented to validate the efficient implementation and accuracy of the proposed method for nonlinear form-finding.

Based on the qualitative knowledge acquired from symmetry analysis, the main contribution of this work is developing a method for the accurate, iterative extraction of nodal coordinate vectors and integral self- stress states from the null space of certain key blocks by a relatively small computational cost. Moreover, to effectively evaluate the null space of the block matrices, the QR decomposition with column pivoting is utilized.

Importantly, the nonlinear form-finding process considers not only the given symmetry and the stability of a structure, but also the uniformity and unilaterality conditions of the members. This method could potentially find applications in the design and optimization of novel tensegrities and prestressed cable–strut structures, as different initial force densities can develop various stable self-equilibrium configurations.

Acknowledgements This work was supported by the National Natural Science Foundation of China (Grant Numbers 51508089 and 51850410513), Southeast University "Zhongying Young Scholars" Project, and the Fundamental Research Funds for the Central Universities. The first author would like to acknowledge financial support from the Alexander von Humboldt Foundation for his visiting research at Max-Planck-Institut für Eisenforschung GmbH, Germany. The last author would like to acknowledge the award of *Research Fund for International Young Scientists* from the National Natural Science Foundation of China. The authors are grateful to the editors and anonymous reviewers for their professional comments and valuable suggestions in improving the quality of the paper.

References

1. Veenendaal, D., Block, P.: An overview and comparison of structural form finding methods for general networks. Int J. Solids Struct **49**, 3741–3753 (2012)
2. Motro, R.: Tensegrity: Structural Systems for the Future Kogan Page Science. Elsevier, London (2003)
3. Wang, B., Guan, S., Zhang, Y., Bai, Y.: Experimental behavior and failure modes of hybrid beam-to-column connections with RC wing-walls in industrial construction. Constr. Build. Mater. **218**, 628–643 (2019)
4. Chen, Y., Feng, J., Zhang, Y.T.: A necessary condition for stability of kinematically indeterminate pin-jointed structures with symmetry. Mech. Res. Commun. **60**, 64–73 (2014)
5. Chen, Y., Yan, J., Sareh, P., Feng, J.: Nodal flexibility and kinematic indeterminacy analyses of symmetric tensegrity structures using orbits of nodes. Int. J. Mech Sci. **155**, 41–49 (2019)
6. Levy, M.P., Jing, T.F.: Floating saddle connections for the Georgia Dome. USA. Struct. Eng. Int. **4**, 148–150 (1994)
7. Zhang, L.Y., Zhu, S.X., Li, S.X., Xu, G.K.: Analytical form-finding of tensegrities using determinant of force–density matrix. Compos. Struct. **189**, 87–98 (2018)
8. Koohestani, K.: On the analytical form-finding of tensegrities. Compos. Struct. **166**, 114–119 (2017)
9. Jordán, T., Recski, A., Szabadka, Z.: Rigid tensegrity labelings of graphs. Eur J. Combin. **30**, 1887–1895 (2009)
10. Connelly, R., Whiteley, W.: Second-order rigidity and prestress stability for tensegrity frameworks. SIAM J. Discrete Math. **9**, 453–491 (1996)
11. Ingber, D.E.: Cell structure and hierarchical systems biology. J. Cell Sci **116**, 1157 (2003)
12. Stamenovic´, D.: Effects of cytoskeletal prestress on cell rheological behavior. Acta Biomater. **1**, 255–262 (2005)
13. Feng, F.: Structural behavior and design methods of Tensegrity domes. J. Constr. Steel Res. **61**, 23–35 (2005)
14. Tran, H.C., Lee, J.: Initial self-stress design of tensegrity grid structures. Comput. Struct. **88**, 558–566 (2010)
15. Koohestani, K., Guest, S.D.: A new approach to the analytical and numerical form-finding of tensegrity structures. Int. J. Solids Struct. **50**, 2995–3007 (2013)
16. Chen, Y., Feng, J., Wu, Y.: Novel form-finding of tensegrity structures using ant colony systems. J. Mech. Robot. Trans. ASME **4**, 1283–1289 (2012)
17. Gasparini, D., Klinka, K.K., Arcaro, V.F.: A finite element for form-finding and static analysis of tensegrity structures. J. Mech. Mater. Struct. **6**, 1239–1253 (2011)
18. Zhang, J.Y., Ohsaki, M.: Adaptive force density method for form-finding problem of tensegrity structures. Int. J. Solids Struct. **43**, 5658–5673 (2006)
19. Feng, X.: The optimal initial self-stress design for tensegrity grid structures. Comput. Struct. **193**, 21–30 (2017)
20. Aloui, O., Flores, J., Orden, D., Rhode-Barbarigos, L.: Cellular morphogenesis of three-dimensional tensegrity structures. Comput. Method Appl. Mech. **346**, 85–108 (2019)
21. Masic, M., Skelton, R.E., Gill, P.E.: Algebraic tensegrity form-finding. Int. J. Solids Struct. **42**, 4833–4858 (2005)
22. Connelly, R., Back, A.: Mathematics and Tensegrity: Group and representation theory make it possible to form a complete catalogue of "strut-cable" constructions with prescribed symmetries. Am. Sci. **86**, 142–151 (1998)
23. Zhang, J.Y., Guest, S.D., Ohsaki, M.: Symmetric prismatic tensegrity structures. Part II: Symmetry-adapted formulations. Int. J. Solids Struct. **46**, 15–30 (2009)
24. Chen, Y., Sun, Q., Feng, J.: Group-theoretical form-finding of cable-strut structures based on irreducible representations for rigid-body translations. Int. J. Mech. Sci. **144**, 205–215 (2018)
25. Chen, Y., Feng, J., Ma, R., Zhang, Y.: Efficient symmetry method for calculating integral prestress modes of statically indeterminate cable-strut structures. J. Struct. Eng. ASCE **141**, 04014240 (2015)
26. Kaveh, A., Daei, M.: Efficient force method for the analysis of finite element models comprising of triangular elements using ant colony optimization. Finite Elem. Anal. Des. **45**, 710–720 (2009)
27. Kaveh, A., Daei, M.: Suboptimal cycle bases of graphs using ant colony system algorithm. Eng. Comput. **27**, 485–494 (2010)
28. Kaveh, A., Bakhshpoori, T.: Metaheuristics: Outlines. MATLAB Codes and Examples. Springer, Switzerland (2019)
29. Rieffel, J., Valero-Cuevas, F., Lipson, H.: Automated discovery and optimization of large irregular tensegrity structures. Comput. Struct. **87**, 368–379 (2009)
30. Lee, S., Woo, B.H., Lee, J.: Self-stress design of tensegrity grid structures using genetic algorithm. Int. J. Mech. Sci. **79**, 38–46 (2014)
31. Koohestani, K.: Form-finding of tensegrity structures via genetic algorithm. Int. J. Solids Struct. **49**, 739–747 (2012)
32. Tran, H.C., Lee, J.: Advanced form-finding of tensegrity structures. Comput. Struct. **88**, 237–246 (2010)

33. Li, Y., Feng, X.Q., Cao, Y.P., Gao, H.: A Monte Carlo form-finding method for large scale regular and irregular tensegrity structures. Int. J. Solids Struct. **47**, 1888–1898 (2010)
34. Xu, X., Wang, Y., Luo, Y.: Finding member connectivities and nodal positions of tensegrity structures based on force density method and mixed integer nonlinear programming. Eng. Struct. **166**, 240–250 (2018)
35. Zingoni, A.: Group-theoretic exploitations of symmetry in computational solid and structural mechanics. Int. J. Numer. Meth. Eng. **79**, 253–289 (2009)
36. Kaveh, A., Rahami, H., Nikbakht, M.: Vibration analysis of regular structures by graph products: cable networks. Comput. Struct. **88**, 588–601 (2010)
37. Chen, Y., Feng, J., Lv, H., Sun, Q.: Symmetry representations and elastic redundancy for members of tensegrity structures. Compos. Struct. **203**, 672–680 (2018)
38. Kaveh, A.: Optimal Analysis of Structures by Concepts of Symmetry and Regularity. Springer, Wien (2013)
39. Chen, Y., Sareh, P., Yan, J., Fallah, A.S., Feng, J.: An integrated geometric-graph-theoretic approach to representing origami structures and their corresponding truss frameworks. J. Mech. Des. Trans. ASME **141**, 091402 (2019)
40. Chen, Y., Feng, J., Sun, Q.: Lower-order symmetric mechanism modes and bifurcation behavior of deployable bar structures with cyclic symmetry. Int. J. Solids Struct. **139–140**, 1–14 (2018)
41. Sareh, P., Guest, S.D.: Designing symmetric derivatives of the Miura-ori. In: Advances in Architectural Geometry, pp. 233–241 (2014)
42. Sareh, P.: Symmetric descendants of the Miura-ori. Engineering Department, University of Cambridge, UK (2014)
43. Pellegrino, S., Tibert, A.G.: Review of form-finding methods for tensegrity structures. Int. J. Space Struct. **18**, 209–223 (2011)
44. Chen, Y., Feng, J.: Generalized eigenvalue analysis of symmetric prestressed structures using group theory. J. Comput. Civil Eng. ASCE **26**, 488–497 (2012)
45. Tran, H.C., Lee, J.: Advanced form-finding for cable-strut structures. Int. J. Solids Struct. **47**, 1785–1794 (2010)
46. Altmann, S.L., Herzig, P.: Point-Group Theory Tables. Clarendon Press, Oxford (1994)
47. Chen, Y., Feng, J.: Efficient method for Moore-Penrose inverse problems involving symmetric structures based on group theory. J. Comput. Civil Eng. ASCE **28**, 182–190 (2014)
48. Katsikis, V.N., Pappas, D., Petralias, A.: An improved method for the computation of the MoorePenrose inverse matrix. Appl. Math. Comput. **217**, 9828–9834 (2011)
49. Zhang, J.Y., Ohsaki, M.: Stability conditions for tensegrity structures. Int. J. Solids Struct. **44**, 3875–3886 (2007)
50. Chen, Y., Feng, J., Wu, Y.: Prestress stability of pin-jointed assemblies using ant colony systems. Mech. Res. Commun. **41**, 30–36 (2012)
51. Motro, R., Vassart, N.: Tensegrity systems. Int. J. Space Struct. **18**, 77–84 (2009)
52. Zhang, J.Y., Ohsaki, M.: Force identification of prestressed pin-jointed structures. Comput. Struct. **89**, 2361–2368 (2011)
53. Kennedy, J.: Particle swarm optimization. In: Encyclopedia of Machine Learning, pp. 760–766. Springer, Berlin (2011)
54. Kaveh, A., Zolghadr, A.: Democratic PSO for truss layout and size optimization with frequency constraints. Comput. Struct. **130**, 10–21 (2014)
55. Kaveh, A., Talatahari, S.: Particle swarm optimizer, ant colony strategy and harmony search scheme hybridized for optimiza- tion of truss structures. Comput. Struct. **87**, 267–283 (2009)
56. Ohsaki, M., Zhang, J., Elishakoff, I.: Multiobjective hybrid optimization-antioptimization for force design of tensegrity structures. J. Appl. Mech. Trans. ASME **79**, 021015 (2012)